Automatic prediction of TMJ disc displacement in CBCT images using machine learning

Hanseung Choi

The Graduate School
Yonsei University
Department of Dentistry

Automatic prediction of TMJ disc displacement in CBCT images using machine learning

A Dissertation Submitted
to the Department of Dentistry
and the Graduate School of Yonsei University
in partial fulfillment of the
requirements for the degree of
Doctor of Philosophy in Applied Life Science

Hanseung Choi

January 2025

This certifies that the Dissertation of Hanseung Choi is approved

Thesis Supervisor Sang-Sun Han

Thesis Committee Member Kug Jin Jeon

Thesis Committee Member Chena Lee

Thesis Committee Member Yoon Joo Choi

Thesis Committee Member Gyu-Dong Jo

The Graduate School
Yonsei University
January 2025

감사의 글

저의 앞길을 예비하시고 대학원 입학부터 졸업까지 모든 과정을 잘 마무리 할 수 있도록 인도해 주신 하나님께 모든 영광을 올려드립니다.

제가 연구자의 길을 걸을 수 있도록 이끌어주시고 아낌없는 관심과 격려로 따뜻하게 지도해 주신 한상선 지도교수님께 마음 깊이 존경과 감사의 인사를 드립니다. 논문을 작성하면서 방향을 잃고 헤맬 때마다 길을 알려주신 전국진 교수님, 항상 온화한 미소로 연구뿐만 아니라 작은 고민까지 보살펴 주시는 이채나 교수님, 놀라운 통찰력으로 세심한 부분까지 조언해 주시는 최윤주 교수님, 논문의 완성도를 위해 함께 고민해 주시고 도움을 주신 조규동 교수님, 늘 응원해 주시고 챙겨주신 김학선 교수님께 감사의 인사를 드립니다.

지혜로운 모습으로 연구원들의 본보기가 되어주신 영현 선생님, 섬세한 배려로 다정하게 챙겨주신 아리 선생님, 흔들릴 때마다 용기를 북돋아주신 은규 선생님, 이제는 생각의 흐름마저 같아진 소울메이트 휘 선생님, 연구실을 밝은 에너지로 가득 채워주는 지윤 선생님, 막내지만 깊은 배려심을 가진 예림 선생님, 행정 업무를 도와준 혜리 선생님. 모두 감사드립니다.

대학교 졸업 후 대학원 진학의 길을 선택한 결정을 언제나 변함없이 믿고 응원해 주며 든든한 버팀목이 되어준 우리 가족! 그 어떤 단어들로 다 표현할 수 없을 만큼 감사하고 사랑합니다. 그리고 나의 소중한 10년 지기 친구들 유리, 수연, 영주, 희윤아. 너희들 덕분에 낯설고 막막했던 서울 생활을 웃음으로 채우며 잘 적응할 수 있었어. 모두들 고마워!

마지막으로 미처 언급하지 못했지만 저를 격려해 주시고 힘이 되어주신 모든 분들께 감사의 마음을 전합니다. 베풀어주신 소중한 마음들을 잊지 않고 나누며 살아가겠습니다.

2025년 1월 저자 씀

TABLE OF CONTENTS

LIST OF FIGURES

LIST OF TABLES

ABSTRACT

Automatic prediction of TMJ disc displacement in CBCT images using machine learning

Purpose: The purpose of this study was to develop a machine learning (ML) model to predict temporomandibular joint (TMJ) disc displacement using radiomics features extracted from cone-beam computed tomography (CBCT) images, without the need for magnetic resonance imaging (MRI).

Methods: A total of 247 mandibular condyle datasets from CBCT images of 134 patients were analyzed in this study. Three experiments were conducted using random forest (RF) and extreme gradient boosting (XGBoost) models to classify TMJ disc displacement based on radiomics features obtained from the condylar head on CBCT. Experiment 1 classified the data into three groups—Normal, disc displacement with reduction (DDWR), and disc displacement without reduction (DDWOR)—based on the stage of TMJ disc displacement. Experiment 2 focused on differentiating the TMJ disc displacement group (DDWR and DDWOR) from the Normal group. Experiment 3 aimed to classify Normal and DDWR as a single group, distinguishing them from DDWOR. The developed models were evaluated using the area under the receiver operating characteristic curve (AUC), accuracy, precision, recall, specificity, and F1-score.

Results: Across all experiments, the RF model outperformed the XGBoost model, with the highest accuracy in Experiment 3, followed by Experiments 2 and 1. In Experiment 3, the RF and XGBoost models classified Normal and DDWR as one group and DDWOR as the other, with AUC values of 0.86 and 0.85, respectively. Experiment 2 classified the Normal group from the combined group DDWR and DDWOR with AUC values of 0.76

for RF and 0.75 for XGBoost. In Experiment 1, which performed the most complex classification into three groups, the RF model achieved an accuracy of 0.63, and the XGBoost model obtained 0.59.

Conclusions: The ML models developed in this study provide a non-invasive approach for predicting TMJ disc displacement using radiomics features extracted from CBCT images. These models offer valuable support as a second opinion for dentists diagnosing TMJ disc displacement and serve as an assisted diagnostic tool when MRI is unavailable.

Key words : Artificial Intelligence, Machine Learning, Cone-Beam Computed Tomography, Temporomandibular Joint, Temporomandibular Joint Disc, Temporomandibular Joint Disorders

1. INTRODUCTION

The temporomandibular joint (TMJ) is a complicated structure where a portion of the temporal bone, the condyle of the mandible, and the articular disc are located (Alomar et al., 2007; Ingawale & Goswami, 2009). The disc, composed of avascular fibrous connective tissue, is between the mandibular condyle and the glenoid fossa (Al-Ani & Gray, 2021; Mallya & Lam, 2018). It translates with the mandible during mouth opening, serving as a shock absorber, thus playing a critical role in the mandibular movement (E Tanaka & Koolstra, 2008; E Tanaka & Van Eijden, 2003). In normal cases, during mouth closing, the borderline of the TMJ disc and thick posterior band are positioned directly superior to the mandibular condyle head. During mouth opening, the thin center part of the disc stays positioned between the condyle head and the articular eminence (Drace & Enzmann, 1990).

It is essential to diagnose disc position in TMJ disorder (TMD) because disc displacement is the common cause of TMD (Young, 2015). Disc displacement can interfere with normal joint function or cause pain, and the progress of inflammation in joint space leads to TMJ dysfunction. TMD often begins with non-specific symptoms such as clicking or joint noises during jaw movement and mild discomfort. As the condition progresses, TMJ disc displacement can be accompanied by hard tissue changes along with a limited range of motion. According to previous studies, there are almost no bony changes in the stage of disc displacement with reduction (DDWR) in which the disc is displaced anteriorly when the mouth is closed. Pathologic bony changes only begin to appear in the intermediate to late stage of TMJ internal derangement (Wilkes, 1989), a case of disc displacement without reduction (DDWOR) in which the disc remains displaced regardless of jaw position (Som & Curtin, 2011).

As TMD progress, limited joint movement leads to dysfunction such as difficulty in eating and talking, and reduces synovial fluid cycling, creating conditions conducive to the accumulation of inflammatory agents. It can also lead to abnormal forces and inflammation

in the joint, resulting in bone changes like flattening, erosion, osteophyte formation, and sclerosis, as well as irregular changes in trabecular pattern (Dias et al., 2012; Roh et al., 2012). Therefore, an accurate diagnosis of disc displacement is important in TMD (Mallya & Lam, 2018).

Panoramic radiograph widely used in dentistry offers a broad coverage of the anatomical structures surrounding the TMJ. However, its limitations as a two-dimensional imaging modality, such as distortion and superimposition of images make it difficult to accurately assess the anatomical structures (Perschbacher, 2012). Cone-beam computed tomography (CBCT) is useful for three-dimensional (3D) evaluating pathologic changes of the bony component of the TMJ structures, but it cannot visualize soft tissue structures such as disc (Honda et al., 2006; Katakami et al., 2008; Mallya & Lam, 2018). Magnetic resonance imaging (MRI) is the most accurate and only non-invasive diagnostic tool for the position and shape of the disc (Emshoff et al., 2002; Larheim, 2005; Sano & Westesson, 1995). It can be taken in closed and opened mouth positions, allowing functional evaluation of disc movement (Brooks & Westesson, 1993; Katzberg et al., 1986). Since MRI uses a large magnet that generates a strong external magnetic field, patients with pacemakers, cerebral aneurysm clips, or cochlea implants cannot undergo MRI, and claustrophobia may also have difficulty with the scan (Mallya & Lam, 2018). Above all, MRI has the disadvantage of being expensive equipment that can only be taken at some hospitals and the cost of taking the scan is also very high.

Due to the limitations of taking an MRI, several studies have attempted to predict TMJ disc displacement using CBCT without MRI. These studies have tried the prediction of disc displacement through joint space alteration, condylar position, and condylar morphology observed on CBCT with clinical symptoms such as pain, sound, and maximum mouth opening range (B. Chen & Li, 2024; Choi & Park, 2016). However, these methods were unable to establish a definitive correlation with disc displacement or emphasized the additional necessity of MRI, and the selection of image slices for evaluation was subjective.

Therefore, in this study, we quantitatively attempted to predict TMJ disc displacement using radiomics data.

Medical images contain various image biomarkers that cannot be perceived by humans but can be used for diagnostic or predictive purposes by converting image data into structured information. Radiomics is one of the image biomarkers frequently used in medical imaging, it can objectively and quantitatively analyze the properties such as shape, texture, and intensity (Jia et al., 2019; Lambin et al., 2012; Mayerhoefer et al., 2020; Rastegar et al., 2020; Tomaszewski & Gillies, 2021). The previous studies, utilized radiomics methods to detect cancer and assess osteoporosis in medical images (He et al., 2019; Jiang et al., 2022; Linning et al., 2019). In the field of dentistry, radiomics features have been used for caries detection, cancer diagnosis, and legal age classification (De Araujo Faria et al., 2021; Fruehwald-Pallamar et al., 2016; Jeon et al., 2023). This study introduces a technique to automatically predict TMJ disc displacement from CBCT images without MRI using two machine learning (ML) models.

Considering the correlation between TMJ disc displacement and changes in the bone marrow and cortical bone of the mandibular condyle, we hypothesized that differences in radiomics features of the condyle head in CBCT images would vary according to the stage of TMJ disc displacement. This study aimed to develop two ML models that utilize only CBCT image radiomics features to predict TMJ disc displacement without MRI.

2. MATERIALS AND METHODS

2.1. Data preparation

This study was approved by the Institutional Review Board (IRB) of Yonsei University Dental Hospital (IRB No. 2-2023-0065). The requirement for patient consent was waived due to the retrospective nature of the image collection, ethical guidelines, and regulations on all methods. All images utilized in the study were anonymized and exported in Digital Image Communication in Medicine format.

Data were collected from patients who visited Yonsei University Dental Hospital from December 2018 to December 2022 and underwent both MRI and CBCT scans. MRI scans were performed with 3.0 T scanner (Pioneer; GE Healthcare, Waukesha, WI, USA) and 16-channel flex large coil. Sagittal section views of the condylar head were acquired using proton density-weighted sequences in the closed-mouth and open-mouth positions with a slice thickness of 2.5 mm. We acquired CBCT scans of each subject using the Alphard 3030 (Asahi Roentgen Ind. Co., Ltd, Kyoto, Japan) machine. The CBCT protocol for TMJ was the field of view 154 × 154 mm, voxel size of 0.3 mm^3, 80 kVp, 8 mAs, and exposure time of 17 s.

The criteria for data collection included: (1) adults aged 20 and older; (2) CBCT images that clearly allowed the identification of the border between the cortical bone and bone marrow of the mandibular condyle; and (3) mandibular condyle of sufficient size to enable 3D manual labeling. Exclusion criteria were as follows: (1) patients with fractures, tumors, or severe anatomical deformities in the TMJ; and (2) CBCT images with significant metal artifacts or severe blurring.

2.2. Three experiments according to classification of TMD groups

Three experiments were performed to predict classification in a total of 247 condylar heads that were collected from 134 patients. The data were randomly selected and adjusted according to group distribution for each experiment (Table 1). An oral radiologist classified the groups by identifying the position of the disc using MRI as the gold standard. Fig. 1 shows examples of TMJ disc positions during the process of opening and closing the mouth for groups divided based on TMJ disc displacement.

(1) Experiment 1: Classification into three groups – Normal vs DDWR vs DDWOR

(2) Experiment 2: Classification into two groups – Normal vs DDWR and DDWOR

(3) Experiment 3: Classification into two groups – Normal and DDWR vs DDWOR

Fig. 2 presents a schema of the proposed study for machine learning-based TMJ disc displacement prediction using radiomics features in the condylar head.

Table 1. Clinical characteristics of three experiments for classifying TMJ disc displacement

		Female	Male	Total
Experiment 1	Normal	51	32	83
	DDWR	59	21	80
	DDWOR	60	24	84
Experiment 2	Normal	51	32	83
	DDWR and DDWOR	47	37	84
Experiment 3	Normal and DDWR	44	39	83
	DDWOR	60	24	84

DDWR, disc displacement with reduction; DDWOR, disc displacement without reduction.

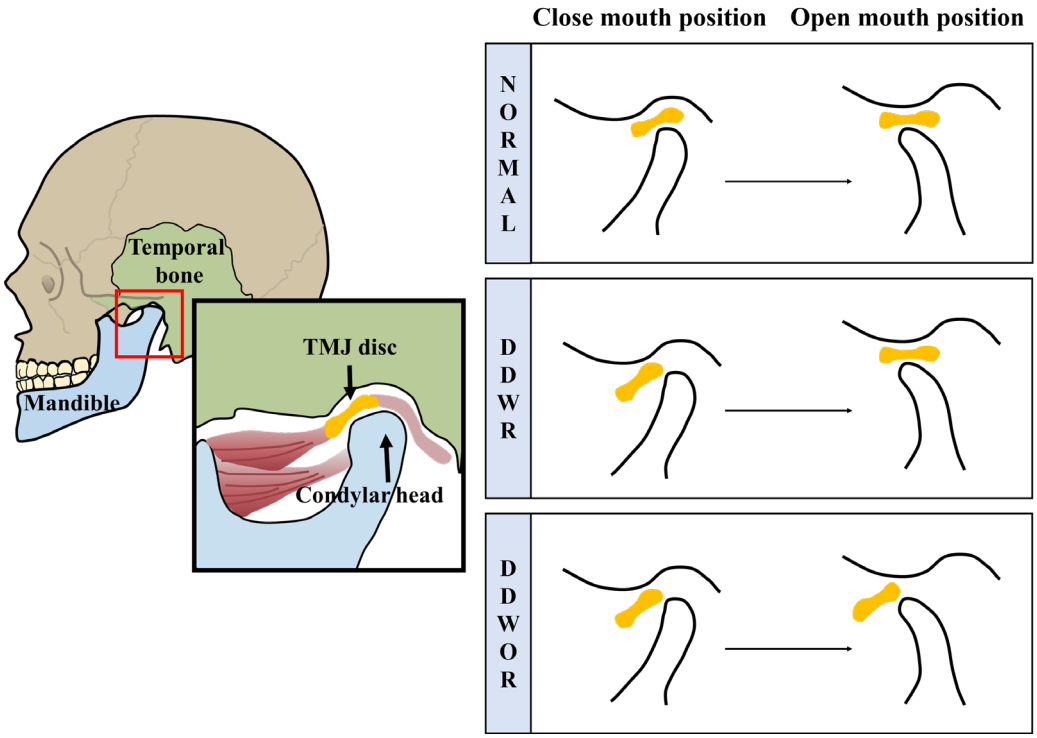

Fig. 1 Examples of TMJ disc position during mouth closing and opening. TMJ, temporomandibular joint; DDWR, disc displacement with reduction, DDWOR, disc displacement without reduction.

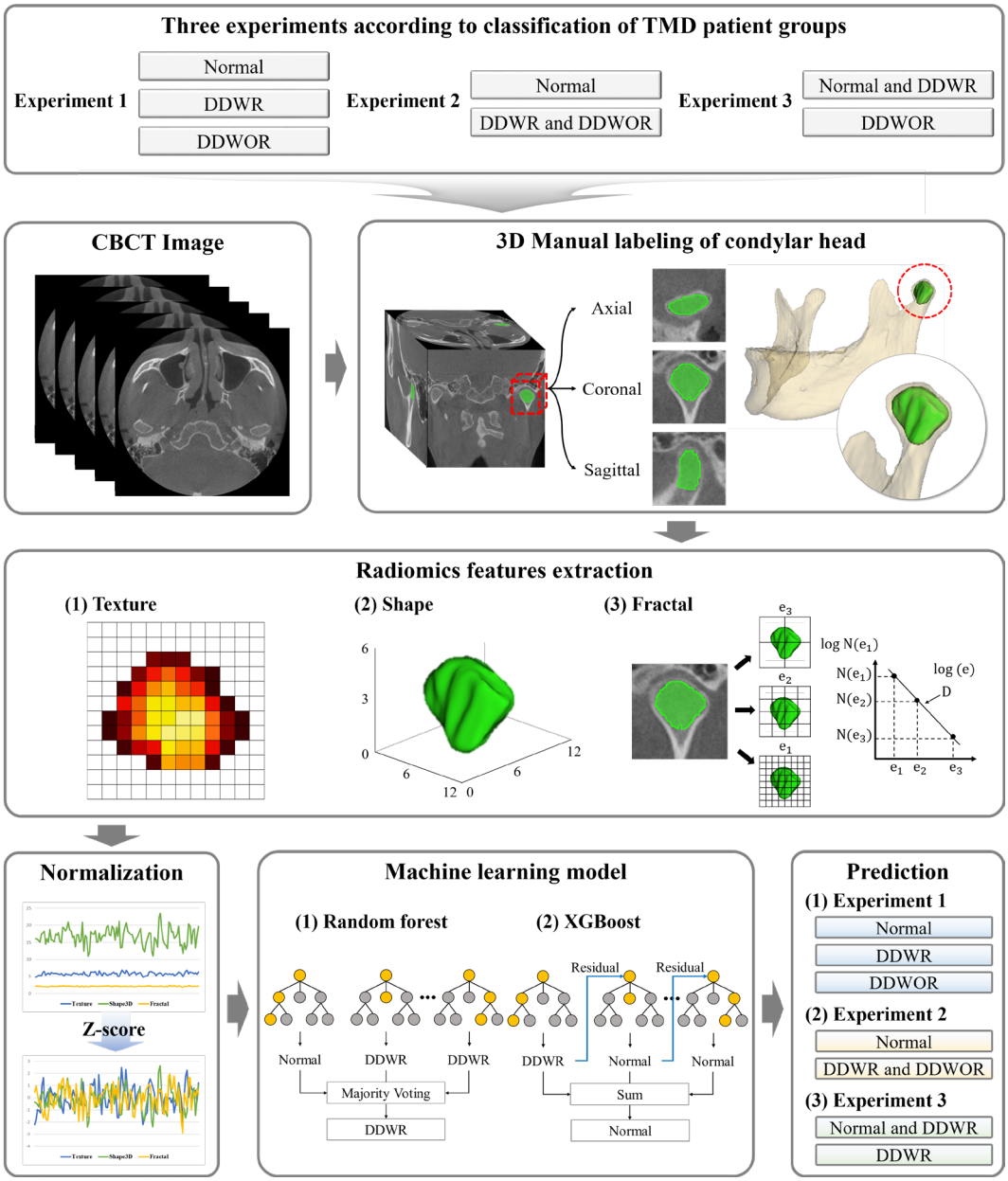

Fig. 2 Overview of machine learning model development for TMJ disc displacement prediction in CBCT images. TMD, temporomandibular joint disorder; TMJ, temporomandibular joint; DDWR, disc displacement with reduction; DDWOR, disc displacement without reduction.

2.3. Segmentation of region of interest in the condylar head in CBCT

The radiomics features were extracted from the CBCT images of the condylar head area, focusing on the bone marrow. In mandibular condyles with erosion and osteophyte formation, the irregular border between bone marrow and cortical bone creates challenges for labeling and can lead to variability among observers. Therefore, the region of interest (ROI) was set in 3D to include the condyle neck of the bone marrow excluding the cortical bone (Fig. 3). The ROI in the TMJ bone marrow was manually segmented using AVIEW research software (Coreline Soft Inc., Seoul, Korea) by an oral radiologist with more than 25 years of experience. An average of 42 CBCT image slices per person were used for condylar head segmentation.

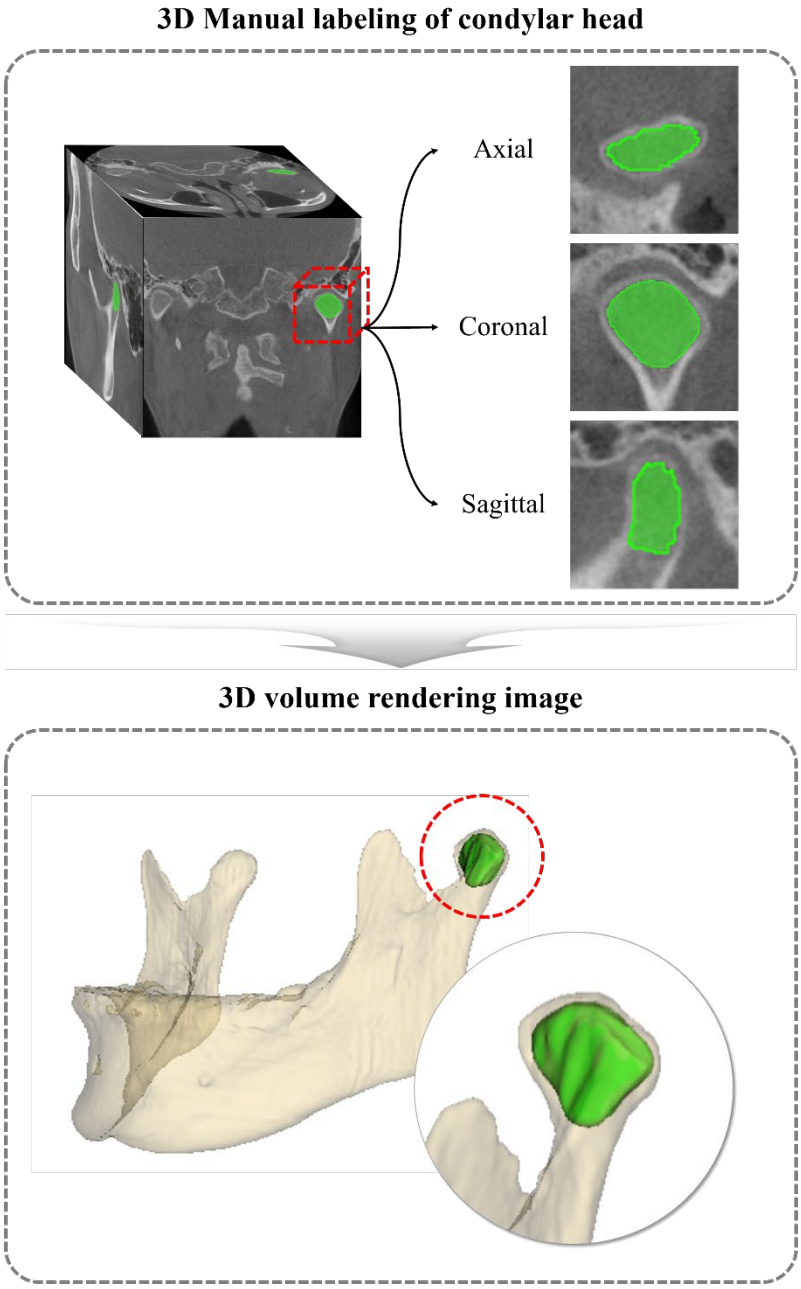

Fig. 3 Process of defining the bone marrow of the mandibular condyle in CBCT images as a three-dimensional region of interest.

2.4. Radiomics features extraction

A total of 132 features were obtained by mathematically quantifying 3D radiomics features from the segmented ROI on CBCT images. The extracted radiomics features were divided into 3 categories: texture, shape, and fractal features (Table 2). The radiomics features were automatically computed through AVIEW research software based on PyRadiomics (https://PyRadiomics.readthedocs.io/en/latest/).

Table 2. Summary of types of radiomics features and descriptions

Radiomics features	Description
Texture	Comprise various statistical information about the gray value distribution inside the ROI. These features included minimum and maximum values of gray level, distribution of voxel intensity, difference values from the neighboring voxels, quantified gray level dependencies, etc.
Shape	Account for geometric properties such as the volume measured by counting the voxel units in the ROI, compactness of the ROI, maximum diameter, maximum surface along various orthogonal directions, and the similarity of the ROI to a sphere, etc.
Fractal	Determine heterogeneity between organizations through pattern difference analysis. Fractal Dimension is a number that quantifies the rate of detailed change due to changes in scale and is easily affected by the shape of the ROI. Using the box-counting slide technique, boxes of various sizes are slid to calculate the fractal dimension of each position. The fractal dimension is defined as the slope of a line.

2.5. Radiomics features normalization

We performed z-score normalization on the extracted feature values for the individual features. Various radiomics features have different units and ranges, some are within the 0 to 1, while others have a much larger range. Without feature normalization, disproportionate weights could be assigned during model training based on the distribution of feature values. Therefore, we applied z-score normalization to ensure that each feature had a relatively consistent range (Fig. 4), and can define it as follows:

$$\text{Normalized Value} = \frac{x-\mu}{\sigma} \quad (1)$$

where x denotes the value to be normalized in the attribute, μ indicates its mean value, and σ is its standard deviation, respectively.

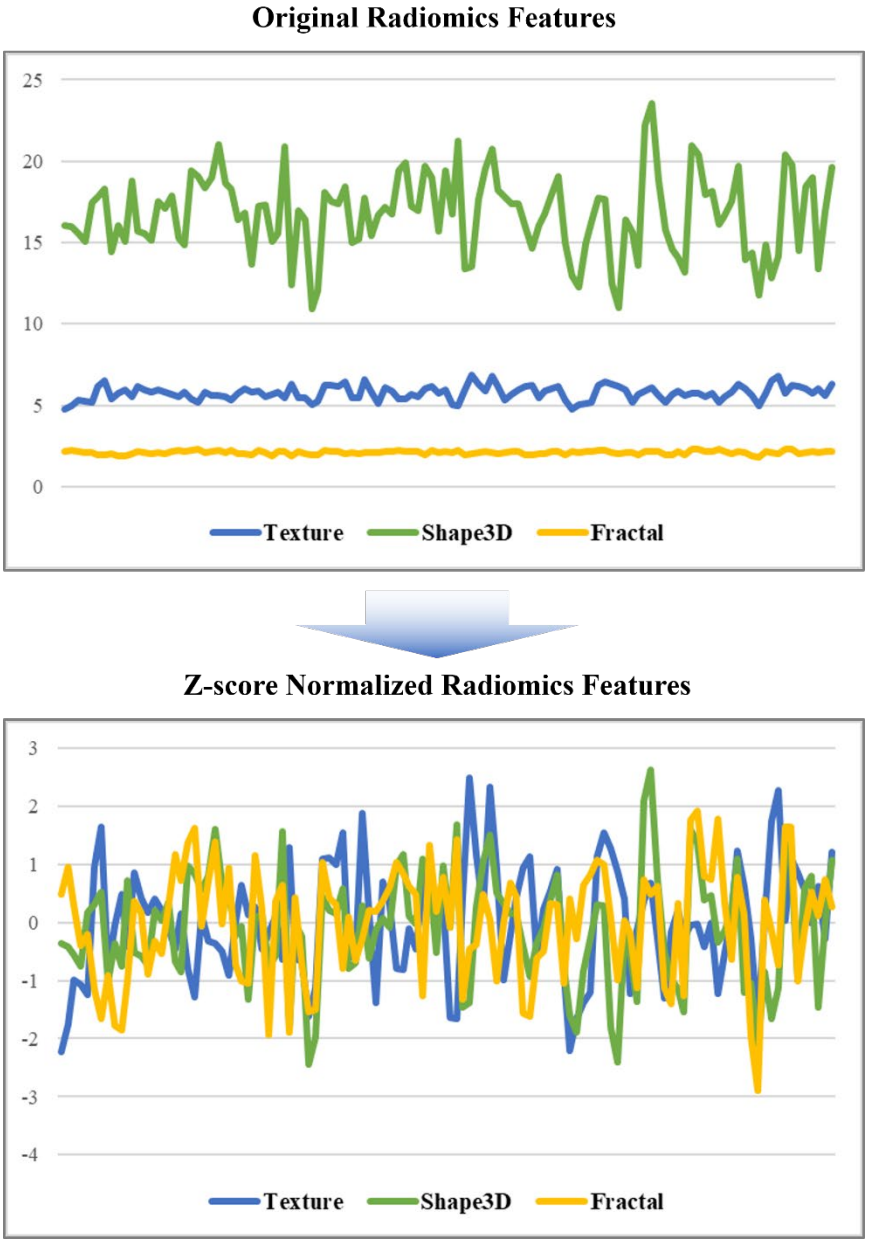

Fig. 4 Changes in radiomics feature values distribution following z-score normalization.

2.6. Machine learning model for TMJ disc displacement prediction

In this study, random forest (RF) and extreme gradient boosting (XGBoost) classifiers were developed to conduct three experiments. These two ML models were implemented using Python language with the scikit-learn package (https://scikit-learn.org/). To train the model, the dataset was divided by 7:3 ratios based on the data class distribution. In Experiment 1, out of 247 condylar heads, 172 were divided as the training data and 75 as the test set. In Experiment 2, 167 condylar heads were divided into 115 for training data and 52 for the test set to evaluate performance. In Experiment 3, 116 condylar heads were used as the training data, and 51 as the test set for the experiment. For both classifiers, we tested a range of tree numbers from 1 to 200 to establish which tree had the highest area under the receiver operating characteristic curve (AUC) value. In the tree model built to obtain the best AUC value, the threshold was adjusted from 0 to 1 to set the parameter to obtain the highest accuracy.

The RF classifier, consisting of several decision trees, mitigates overfitting by training each tree on a subset of the entire dataset (Breiman, 2001). The Gini index, which evaluates the probability of misclassification for each feature in a node, was computed at each node split within RF, reflecting how effectively the data can be categorized within each individual tree. In prediction for a new case, each decision tree casts a vote for a group class, and the votes of all trees in the forest are accumulated to determine the patient's class probability.

XGBoost, introduced by Chen and Guestrin, is a decision tree-based ensemble method and operates within the gradient boosting framework (T. Chen & Guestrin, 2016). This algorithm is an ensemble learning, collecting predictions from multiple weaker learners and determining the final model through a voting process. Unlike the RF classifier, XGBoost has an advantage in producing a robust classification tree, with the loss gradually

decreasing as the weight coefficients for individually weak classifiers are applied to the next decision tree.

2.7. Performance evaluation for prediction models

We calculated the AUC, accuracy, precision, recall, specificity, and F1 score to evaluate the classification performance of RF and XGBoost in predicting TMJ disc displacement using radiomics features. The receiver operating characteristic (ROC) curve is a graph that shows the true positive rate relative to the false positive rate by varying the discriminant threshold, and the AUC refers to the area under this curve. AUC is a value ranging from 0 to 1, with values closer to 1 indicating that the model classified the data perfectly. Python (Python Software Foundation, Version 3.6.1; Wilmington, DE, USA) was utilized to visualize and calculate classification performance. These evaluation measurements are defined as follows:

$$\text{Accuracy} = \frac{TP+TN}{TP+TN+FP+FN} \quad (2)$$

$$\text{Precision} = \frac{TP}{TP+FP} \quad (3)$$

$$\text{Recall} = \frac{TP}{TP+FN} \quad (4)$$

$$\text{Specificity} = \frac{TN}{TN+FP} \quad (5)$$

$$\text{F1 score} = \frac{2*\text{Precision}*\text{Recall}}{\text{Precision}+\text{Recall}} \quad (6)$$

where TP, TN, FP, and FN denote the true positive, true negative, false positive, and false negative, respectively.

3. RESULTS

Overall, the RF model outperformed XGBoost in all three experiments. In Experiment 1, RF and XGBoost models classified Normal, DDWR, and DDWOR with accuracies of 0.63 and 0.59 respectively. The average precision, recall, specificity, and F1 score across the three classes for the RF model were 0.65, 0.62, 0.81, and 0.63. For the XGBoost model, these values were 0.60, 0.59, 0.79, and 0.59, respectively (Table 3, Fig. 5).

In Experiment 2, RF and XGBoost classified Normal and the combined group of DDWR and DDWOR with AUC values of 0.76 and 0.75. For RF, the evaluation metrics were 0.71 (accuracy), 0.72 (precision), 0.69 (recall), 0.73 (specificity), and 0.70 (F1 score), while XGBoost was 0.69, 0.67, 0.77, 0.62, and 0.72 for these metrics, respectively (Table 4, Fig. 6).

In Experiment 3, which classified Normal and DDWR combined group versus DDWOR, both models achieved their highest predictive performance, with all evaluation metrics exceeding 0.80. The RF model reached an AUC of 0.86, accuracy of 0.82, precision of 0.84, recall of 0.81, specificity of 0.84, and F1 score of 0.82. XGBoost achieved 0.85, 0.80, 0.81, 0.81, 0.80, and 0.81 for each evaluation metric (Table 5, Fig. 7).

Table 3. Prediction performance comparison of two ML models in Experiment 1

ML model	Accuracy	Precision	Recall	Specificity	F1score
RF	0.63	0.65	0.62	0.81	0.63
XGBoost	0.59	0.60	0.59	0.79	0.59

ML, machine learning; RF, random forest; XGBoost, extreme gradient boosting.

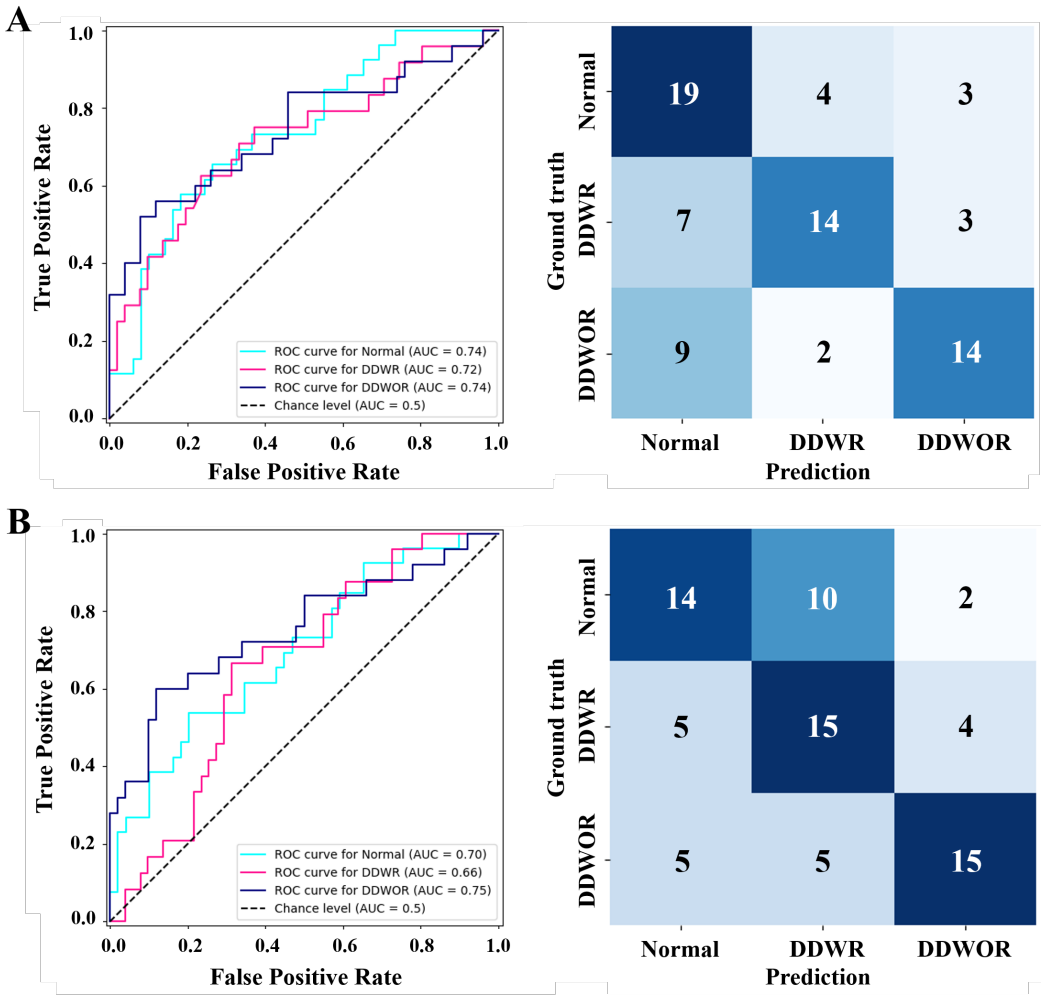

Fig. 5 Receiver operating characteristic curve and confusion matrix of Experiment 1. (A) Random forest. (B) XGBoost. DDWR, disc displacement with reduction; DDWOR, disc displacement without reduction.

Table 4. Prediction performance comparison of two ML models in Experiment 2

ML model	AUC	Accuracy	Precision	Recall	Specificity	F1score
RF	0.76	0.71	0.72	0.69	0.73	0.70
XGBoost	0.75	0.69	0.67	0.77	0.62	0.72

ML, machine learning; RF, random forest; XGBoost, extreme gradient boosting; AUC, area under the curves.

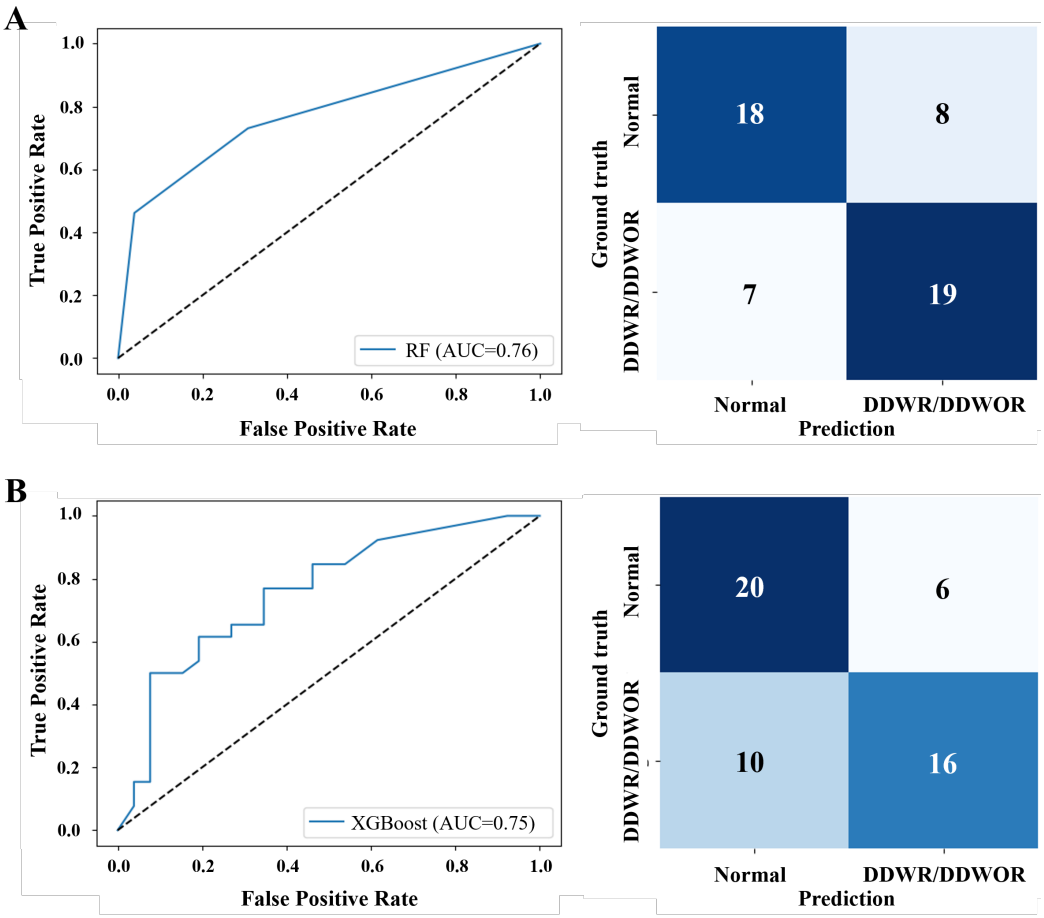

Fig. 6 Receiver operating characteristic curve and confusion matrix of Experiment 2. (A) Random forest. (B) XGBoost. DDWR, disc displacement with reduction; DDWOR, disc displacement without reduction.

Table 5. Prediction performance comparison of two ML models in Experiment 3

ML model	AUC	Accuracy	Precision	Recall	Specificity	F1score
RF	0.86	0.82	0.84	0.81	0.84	0.82
XGBoost	0.85	0.80	0.81	0.81	0.80	0.81

ML, machine learning; RF, random forest; XGBoost, extreme gradient boosting; AUC, area under the curves.

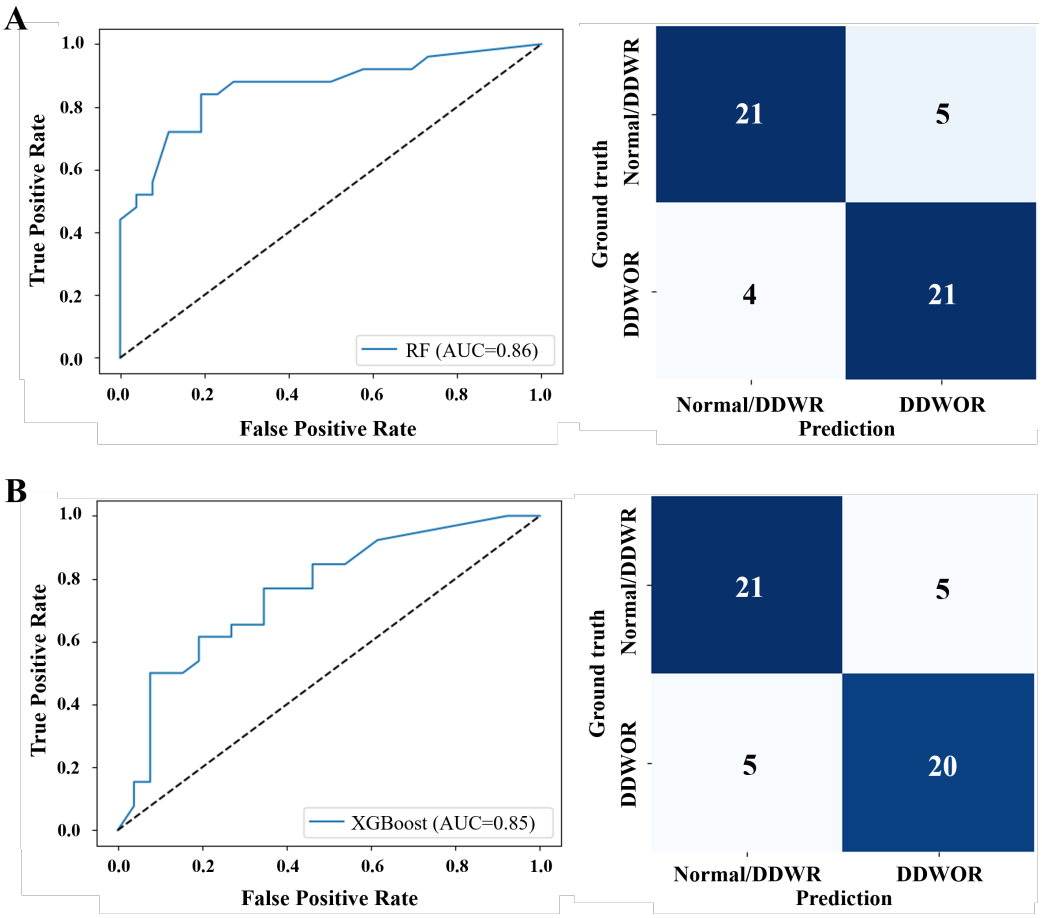

Fig. 7 Receiver operating characteristic curve and confusion matrix of Experiment 3. (A) Random forest. (B) XGBoost. DDWR, disc displacement with reduction; DDWOR, disc displacement without reduction.

In Experiment 3, which achieved the highest accuracy among the three experiments, feature importance was analyzed for the prediction of TMJ disc displacement groups by the two ML models and identified the top 10 features. The features that primarily influenced the classification of Normal and DDWR as a single group versus DDWOR were mainly shape features, and within the texture features, gray-level co-occurrence matrix (GLCM) and gray-level dependence matrix (GLDM) (Fig. 8).

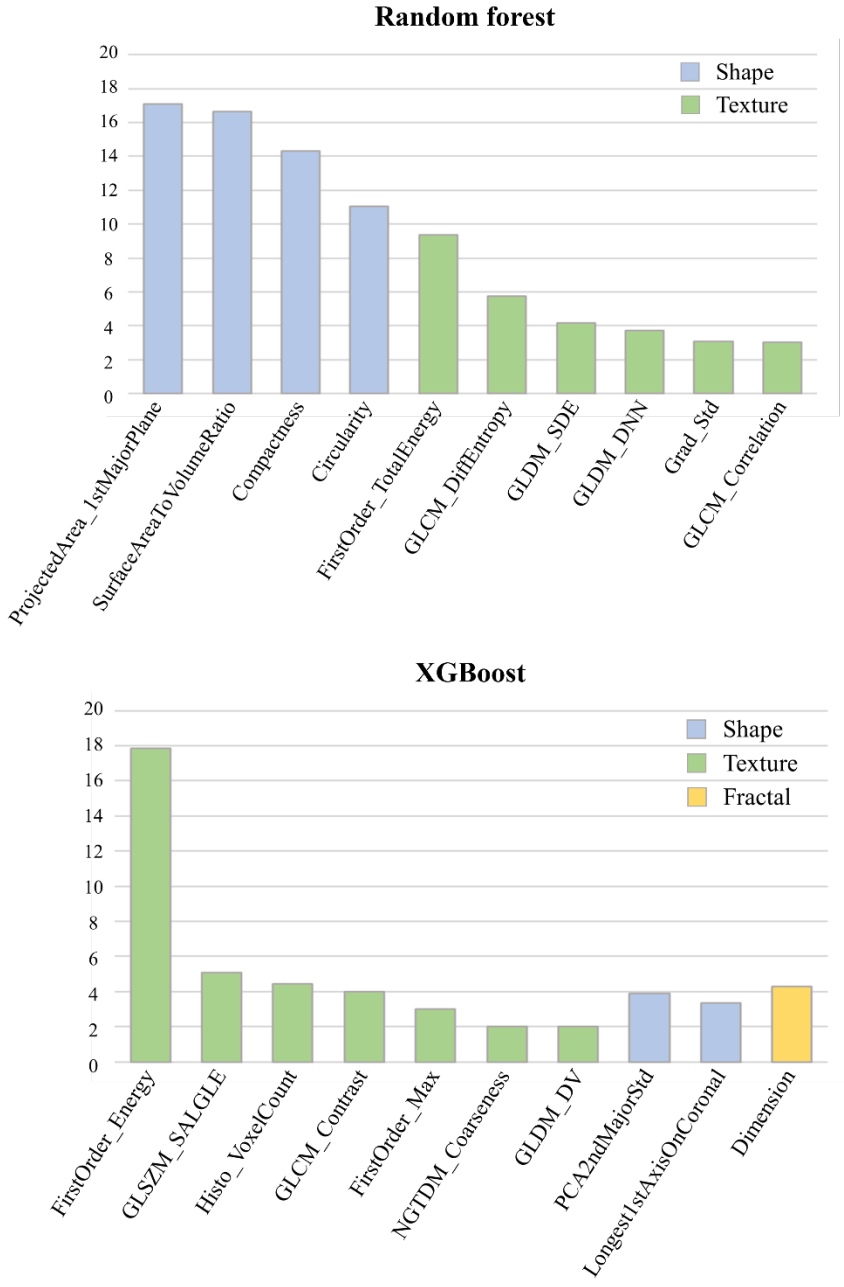

Fig. 8 Top 10 important features of Random forest and XGBoost models in Experiment 3.

4. DISCUSSION

In this study, we proposed two ML models to predict TMJ disc displacement without MRI only using CBCT images. The experimental results demonstrated that the developed model was effective and accurate in classifying the stage of TMJ disc displacement using radiomics features of TMJ bone marrow. Notably, in Experiment 3, where both models showed potential for clinical application in predicting DDWOR among the stages of TMJ disc displacement. According to this experiment, the two ML models can provide objective second opinions to dentists for diagnosing TMJ disc displacement by utilizing radiomics features obtained from the mandibular condyle in CBCT images. Furthermore, these models can serve as non-invasive diagnostic support tools in cases where MRI cannot be performed.

TMD is a disease that causes abnormal joint function due to abnormalities in the position and shape of the disc (Young, 2015). The normal position of the disc is between the mandibular condyle and the articular fossa, but in DDWR, the disc is displaced anteriorly when the mouth is closed. If DDWR is not properly managed, it can progress to DDWOR. When in a closed state compared to DDWR, the disc can be displaced more anteriorly, and when the mouth is opened, the disc does not return to its normal position and is still in front (Som & Curtin, 2011). This condition requires management because it usually causes functional impairment, including the mouth not opening sufficiently and restricting the mandible's movement, making eating and speaking difficult. The shape of a chronically displaced articular disc may become thickened or distorted, and restricted joint movement reduces synovial fluid circulation, creating conditions conducive to the accumulation of inflammatory substances. Therefore, accurate diagnosis and timely management are essential to prevent the progression of the disease.

To diagnose TMD, it is necessary to identify the position of the disc when opening and closing the mouth through MRI (Emshoff et al., 2002; Katzberg et al., 1986). A

patient's clinical symptoms can be varied and sometimes inconsistent, and complex etiologic factors exist, MRI that can detect soft tissue pathology is generally essential (Larheim, 2005). However, MRI is more expensive to purchase and maintain than other dental imaging equipment, so its adoption rate in local hospitals other than university hospitals is low. Additionally, MRI obtains images by positioning the patient within a large magnet, which can be challenging for individuals with pacemakers or claustrophobia (Mallya & Lam, 2018). Therefore, MRI is the most accurate method to diagnose TMJ disc displacement, but its accessibility is low compared to other dental imaging.

Due to the limited accessibility of MRI, previous studies have attempted to diagnose TMJ disc displacement using CBCT without MRI. Choi, H. M., et al. aimed to compare Normal and TMJ disc displacement by analyzing the size and morphology of the mandibular condyle such as condylar height and intercondylar angle on CBCT images (Choi & Park, 2016). However, this analysis method could not find a relationship between the two groups. Chen, B., & Li, C. et al. attempted to determine the relationship between disc position, joint space, and condylar morphology (B. Chen & Li, 2024). However, it was difficult to predict disc shape and position using only CBCT images, and the need for MRI was mentioned. Moreover, the previously mentioned methods rely on a subjective selection of CBCT slices when measuring joint space or condylar angles, which may result in low inter-observer reliability. In contrast, this study proposed a method to classify TMJ disc displacement as a quantitative value by analyzing radiomics features of CBCT images, showing high accuracy with an AUC value of 0.86 to differentiate Normal and DDWR groups from the DDWOR group.

Radiomics enables the quantitative analysis of image features that cannot be observed by the human eye in medical images such as CBCT or MRI (Lambin et al., 2012; Mayerhoefer et al., 2020). The main advantage of radiomics is that it can noninvasively offer valuable information for the diagnosis and prognosis of diseases. This study developed an ML model to predict disc displacement from CBCT images without needing MRI, utilizing the advantage of the radiomics features. In Experiment 1, we aimed to

classify three groups of disc displacement: Normal, DDWR, and DDWOR. The RF and XGBoost classified the three groups with 0.63 and 0.59 accuracy, respectively. In Experiment 2, the objective was to classify Normal and the combination of DDWR and DDWOR, and RF and XGBoost obtained AUC values of 0.76 and 0.75, respectively. In Experiment 3, Normal and DDWR were grouped into one group, while DDWOR was classified into a separate group. The developed RF and XGBoost classified two groups with AUC values of 0.86 and 0.85, respectively.

Compared with Experiment 3, Experiments 1 and 2 achieved relatively low classification accuracies. According to Wilkes' classification of internal derangement of the TMJ shows that no significant changes in hard tissue occur until the middle stage, with pathological alterations in hard tissue beginning in the intermediate-to-late stage (Wilkes, 1989). In this study, the ROI was set in the bone marrow, excluding the cortical bone, to extract radiomics features. Considering this, the radiomics features extracted from the bone marrow of the mandibular condyle may exhibit differences primarily in the stage of DDWOR, which could explain why Experiment 3 achieved the highest accuracy.

In Experiment 3, an analysis of feature importance influencing the classification of Normal and DDWR as one group and DDWOR as the other by two ML models, the top 10 important features were primarily the shape features and, particularly within the texture features, the GLCM and GLDM. The progression of disc displacement from Normal to DDWR and then to DDWOR can lead to abnormal forms of the osseous or soft tissue structures of the joint, such as bone deformities and remodeling, so it is reasonable to accept the influence of shape features. GLCM and GLDM include features that capture the relational information about pixels with similar values within an image and quantify gray-level dependencies between image pixels, respectively. As TMJ disc displacement progresses, the trabecular pattern of the bone marrow becomes more irregular, and these changes may have affected the two features.

The ML models developed in this study demonstrated their potential for clinical application by predicting DDWOR with an AUC value of 0.86 through the analysis of radiomics features of bone marrow. This approach can be applied to patients who cannot undergo MRI and can assist clinicians in treatment planning by providing additional information on disc position, beyond bone changes.

Our model has several considerations that could be improved in future research to achieve better performance. First, CBCT images inherently contain more artifacts than multi-detector CT images due to the lower energy spectrum used. Additionally, the geometric characteristics of image acquisition generate significant scatter radiation, which increases noise in the image. Since noise is a crucial factor in determining image quality, applying the developed method to images acquired with higher resolution and state-of-the-art equipment is expected to yield improved results. Second, this study’s data were collected from a single institution. Therefore, if future research utilizes multi-institutional imaging, a more generalized and reliable model could be developed. Addressing these issues could improve the model's accuracy in classifying Normal, DDWR, and DDWOR into three groups.

5. CONCLUSION

This study developed ML-based models to predict TMJ disc displacement by analyzing radiomics features of the condylar head in CBCT images and demonstrated their potential for clinical application. These models can offer a second opinion to novice dentists diagnosing TMJ disc displacement and can be utilized as an assisted diagnostic tool when MRI is not feasible.

REFERENCES

Al-Ani, Z., & Gray, R. J. (2021). *Temporomandibular disorders: a problem-based approach*: John Wiley & Sons. 11-14.

Alomar, X., Medrano, J., Cabratosa, J., Clavero, J., Lorente, M., Serra, I., . . . Salvador, A. (2007). *Anatomy of the temporomandibular joint.* Paper presented at the Seminars in Ultrasound, CT and MRI.

Breiman, L. (2001). Random forests. *Machine learning, 45*, 5-32.

Brooks, S. L., & Westesson, P.-L. (1993). Temporomandibular joint: value of coronal MR images. *Radiology, 188*(2), 317-321.

Chen, B., & Li, C. (2024). The relationship between the articular disc in magnetic resonance imaging and the condyle in cone beam computed tomography: a retrospective study. *Journal of Stomatology, Oral and Maxillofacial Surgery*, 101940.

Chen, T., & Guestrin, C. (2016). *Xgboost: A scalable tree boosting system.* Paper presented at the Proceedings of the 22nd acm sigkdd international conference on knowledge discovery and data mining.

Choi, H.-M., & Park, M.-S. (2016). Cone-Beam Computed Tomographic Assessment of Temporomandibular Joint Morphology in Patients with Temporomandibular Joint Disc Displacement and in Healthy Subjects: A Pilot Study: A Pilot Study. *Journal of Oral Medicine and Pain, 41*(2), 41-47.

De Araujo Faria, V., Azimbagirad, M., Viani Arruda, G., Fernandes Pavoni, J., Cezar Felipe, J., dos Santos, E. M. C. M. F., & Murta Junior, L. O. (2021). Prediction of radiation-related dental caries through pyradiomics features and artificial neural network on panoramic radiography. *Journal of Digital Imaging, 34*, 1237-1248.

Dias, I. M., Coelho, P. R., Assis, N. M. S. P., Leite, F. P. P., & Devito, K. L. (2012). Evaluation of the correlation between disc displacements and degenerative bone changes of the temporomandibular joint by means of magnetic resonance images. *International journal of oral and maxillofacial surgery, 41*(9), 1051-1057.

Drace, J. E., & Enzmann, D. R. (1990). Defining the normal temporomandibular joint: closed-, partially open-, and open-mouth MR imaging of asymptomatic subjects. *Radiology, 177*(1),

67-71.

Emshoff, R., Rudisch, A., Innerhofer, K., Brandlmaier, I., Moschen, I., & Bertram, S. (2002). Magnetic resonance imaging findings of internal derangement in temporomandibular joints without a clinical diagnosis of temporomandibular disorder. *Journal of oral rehabilitation, 29*(6), 516-522.

Fruehwald-Pallamar, J., Hesselink, J., Mafee, M., Holzer-Fruehwald, L., Czerny, C., & Mayerhoefer, M. (2016). *Texture-based analysis of 100 MR examinations of head and neck tumors–is it possible to discriminate between benign and malignant masses in a multicenter trial?* Paper presented at the RöFo-Fortschritte auf dem Gebiet der Röntgenstrahlen und der bildgebenden Verfahren.

He, B., Ji, T., Zhang, H., Zhu, Y., Shu, R., Zhao, W., & Wang, K. (2019). MRI-based radiomics signature for tumor grading of rectal carcinoma using random forest model. *Journal of cellular physiology, 234*(11), 20501-20509.

Honda, K., Larheim, T., Maruhashi, K., Matsumoto, K., & Iwai, K. (2006). Osseous abnormalities of the mandibular condyle: diagnostic reliability of cone beam computed tomography compared with helical computed tomography based on an autopsy material. *Dentomaxillofacial Radiology, 35*(3), 152-157.

Ingawale, S., & Goswami, T. (2009). Temporomandibular joint: disorders, treatments, and biomechanics. *Annals of biomedical engineering, 37*, 976-996.

Jeon, K. J., Kim, Y. H., Choi, H., Ha, E.-G., Jeong, H., & Han, S.-S. (2023). Radiomics approach to the condylar head for legal age classification using cone-beam computed tomography: A pilot study. *PLoS One, 18*(1), e0280523.

Jia, T.-Y., Xiong, J.-F., Li, X.-Y., Yu, W., Xu, Z.-Y., Cai, X.-W., . . . Zhang, J. (2019). Identifying EGFR mutations in lung adenocarcinoma by noninvasive imaging using radiomics features and random forest modeling. *European radiology, 29*, 4742-4750.

Jiang, Y.-W., Xu, X.-J., Wang, R., & Chen, C.-M. (2022). Radiomics analysis based on lumbar spine CT to detect osteoporosis. *European radiology, 32*(11), 8019-8026.

Katakami, K., Shimoda, S., Kobayashi, K., & Kawasaki, K. (2008). Histological investigation of osseous changes of mandibular condyles with backscattered electron images. *Dentomaxillofacial Radiology, 37*(6), 330-339.

Katzberg, R. W., Bessette, R. W., Tallents, R. H., Plewes, D., Manzione, J., Schenck, J., . . . Hart, H.

(1986). Normal and abnormal temporomandibular joint: MR imaging with surface coil. *Radiology, 158*(1), 183-189.

Lambin, P., Rios-Velazquez, E., Leijenaar, R., Carvalho, S., Van Stiphout, R. G., Granton, P., . . . Dekker, A. (2012). Radiomics: extracting more information from medical images using advanced feature analysis. *European journal of cancer, 48*(4), 441-446.

Larheim, T. A. (2005). Role of magnetic resonance imaging in the clinical diagnosis of the temporomandibular joint. *Cells Tissues Organs, 180*(1), 6-21.

Linning, E., Lu, L., Li, L., Yang, H., Schwartz, L. H., & Zhao, B. (2019). Radiomics for classification of lung cancer histological subtypes based on nonenhanced computed tomography. *Academic radiology, 26*(9), 1245-1252.

Mallya, S., & Lam, E. (2018). *White and Pharoah's oral radiology: principles and interpretation*: Elsevier Health Sciences. 576-593.

Mayerhoefer, M. E., Materka, A., Langs, G., Häggström, I., Szczypiński, P., Gibbs, P., & Cook, G. (2020). Introduction to radiomics. *Journal of Nuclear Medicine, 61*(4), 488-495.

Perschbacher, S. (2012). Interpretation of panoramic radiographs. *Australian dental journal, 57*, 40-45.

Rastegar, S., Vaziri, M., Qasempour, Y., Akhash, M., Abdalvand, N., Shiri, I., . . . Zaidi, H. (2020). Radiomics for classification of bone mineral loss: a machine learning study. *Diagnostic and interventional imaging, 101*(9), 599-610.

Roh, H.-S., Kim, W., Kim, Y.-K., & Lee, J.-Y. (2012). Relationships between disk displacement, joint effusion, and degenerative changes of the TMJ in TMD patients based on MRI findings. *Journal of Cranio-Maxillofacial Surgery, 40*(3), 283-286.

Sano, T., & Westesson, P.-L. (1995). Magnetic resonance imaging of the temporomandibular joint: increased T2 signal in the retrodiskal tissue of painful joints. *Oral Surgery, Oral Medicine, Oral Pathology, Oral Radiology, and Endodontology, 79*(4), 511-516.

Som, P. M., & Curtin, H. D. (2011). *Head and neck imaging: expert consult-online and print*: Elsevier Health Sciences. 1547-1553.

Tanaka, E., & Koolstra, J. (2008). Biomechanics of the temporomandibular joint. *Journal of dental research, 87*(11), 989-991.

Tanaka, E., & Van Eijden, T. (2003). Biomechanical behavior of the temporomandibular joint disc. *Critical Reviews in Oral Biology & Medicine, 14*(2), 138-150.

Tomaszewski, M. R., & Gillies, R. J. (2021). The biological meaning of radiomic features. *Radiology, 298*(3), 505-516.

Wilkes, C. H. (1989). Internal derangements of the temporomandibular joint: pathological variations. *Archives of otolaryngology–head & neck surgery, 115*(4), 469-477.

Young, A. L. (2015). Internal derangements of the temporomandibular joint: A review of the anatomy, diagnosis, and management. *The Journal of Indian Prosthodontic Society, 15*(1), 2-7.

ABSTRACT IN KOREAN

콘빔전산화단층영상 내 라디오믹스 데이터를 이용한 턱관절 관절원판 변위 예측 머신러닝 모델 개발

연구목적: 본 연구의 목적은 자기공명영상 없이 콘빔전산화단층영상 내 하악과두에서 획득한 라디오믹스 데이터를 이용하여 턱관절 관절원판 변위를 예측하는 머신러닝 모델을 개발하고자 한다.

연구대상 및 방법: 2018 년 12 월부터 2022 년 12 월까지 연세대학교 치과병원을 내원하여 자기공명영상과 콘빔전산화단층영상을 모두 촬영한 134 명의 환자로부터 247 개의 하악과두 데이터를 수집했다. 영상치의학 전문의가 자기공명영상에서 턱관절 관절원판 변위 여부를 판독하여 그룹을 분류한 후, 콘빔전산화단층영상 내 하악과두의 해면골에서 3 차원으로 관심영역을 설정하여 132 개의 라디오믹스 데이터를 추출하였다. 추출된 라디오믹스 데이터를 사용하여 턱관절 관절원판 변위를 예측하기 위해 머신러닝 모델인 Random forest (RF)와 XGBoost 를 구축하여 세 가지 실험을 진행하였으며, 각 실험 진행에 따라 그룹별 데이터 분포를 조정하였다.

- 실험 1: 정상, 정복성 관절원판 변위, 비정복성 관절원판 변위 분류
- 실험 2: 정상 vs 정복성 관절원판 변위 및 비정복성 관절원판 변위 분류
- 실험 3: 정상 및 정복성 관절원판 변위 vs 비정복성 관절원판 변위 분류

개발된 모델의 턱관절 관절원판 변위 분류 성능 평가를 위해 수신자 조작 특성 곡선의 아래 면적 값(AUC), 정확도, 정밀도, 재현율, 특이도, F1 점수 평가지표를 이용하였다.

연구결과: 모든 실험에서 RF 모델 성능이 XGBoost 모델보다 우수했으며 실험 3 에서 정확도가 가장 높았고 실험 2 와 실험 1 의 순으로 성능이 우수했다. 실험 3 에서 RF 와 XGBoost 모델은 각각 AUC 값 0.86 과 0.85 로 정상 및 정복성 관절원판 변위 그룹을 비정복성 관절원판 변위 그룹과 분류하였다. 실험 2 에서는 RF 와 XGBoost 모델이 정상 그룹과 정복성 관절원판 변위 및 비정복성 관절원판 변위 그룹을 각각 AUC 값 0.76 과 0.75 로 분류하였다. 분류 클래스 수가 세 그룹으로 가장 많은 실험 1 에서 RF 모델은 정확도 0.63, XGBoost 모델은 정확도 0.59 를 획득하였다.

결론: 본 연구에서는 콘빔전산화단층영상 내 하악과두의 해면골에서 획득한 라디오믹스 데이터 분석을 통해 턱관절 관절원판 변위를 예측할 수 있는 머신러닝 모델을 개발하고 임상적 활용 가능성을 보여주었다. 그러나 실험 1 과 실험 2 에서 턱관절 관절원판 변위 분류 정확도는 높지 않았다. 이는 턱관절 질환의 중, 후기 단계에서 경조직에 병리학적 변화가 발생하는 점을 고려하였을 때 하악과두 해면골에서 얻은 라디오믹스 데이터는 비정복성 관절원판 변위 단계에 이르렀을 때 특징 값의 차이가 나타났을 가능성이 있으며, 이것이 실험 3 의 정확도가 가장 높은 이유로 예상할 수 있다.

본 연구에서 개발된 머신러닝 모델은 턱관절 관절원판 변위 진단 시 치과의사에게 객관적인 2 차 의견을 제공할 수 있으며, 자기공명영상 촬영이 어려운 경우 비침습적인 보조 진단 수단으로 활용될 수 있다.

핵심되는 말: 인공지능, 머신러닝, 콘빔전산화단층영상, 측두하악관절, 턱관절 관절원판, 측두하악관절 장애